PAPER

Check for updates

Passivation of precipitation-hardened UNS N07718 in a shallow sour aqueous solution

Jun-Seob Lee, [ID] *[ab] Ye-Jin Lee,[b] Soon il Kwon,[c] Jungho Shin,[c] Sung Kang,[d] Seung-Hoon Baek[d] and Je-Hyun Lee[ab]

Passivation of precipitation-hardened UNS N07718 in 5 wt% NaCl + 0.5 wt% CH_3COOH was investigated. Cyclic potentiodynamic polarisation revealed that the alloy surface was passivated without active-passive transition behaviour. The alloy surface was in a stable passive state during potentiostatic polarisation at 0.5 V_{SSE} for 12 h. Bode and Mott–Schottky plots showed that the passive film became electrically resistive and less defective with n-type semiconductive properties during the polarisation. X-ray photoelectron spectra revealed that Cr- and Fe-enriched hydro/oxide layers were formed on the outer and inner layers of the passive film, respectively. The thickness of the film was almost constant with the increase of the polarisation time. The outer Cr-hydroxide layer changed into a Cr-oxide layer during the polarisation, resulting in a decreased donor density in the passive film. The film's composition change during the polarisation should be related to the corrosion resistance of the alloy in the shallow sour conditions.

1. Introduction

UNS N07718, a nickel-based alloy that can be precipitation-hardened, is widely used because of its high strength and corrosion resistance in aqueous environments, such as in oil-field, marine, and high-temperature applications.[1–4] The UNS N07718 alloy is corrosion-resistive in oil fields, such as fasteners, bolts, and nuts, where a shallow sour (sweet) condition is associated with the localised corrosion.[5,6] The sweet wells are mildly corrosive to Ni-based alloys due to the passive film on the alloy surfaces, which governs the localised corrosion resistance during service in the environments. For these reasons, the precipitation-hardened UNS N07718 alloy provides the desired mechanical properties[7,8] and localised corrosion resistance in sour environments.[4]

Understanding the electrochemical properties of the passive film formed on the surface of the alloy exposed to corrosive environments is necessary, because the localised corrosion resistance of the UNS N07718 alloy is strongly related to these properties. Some researchers have demonstrated the composition[2] and electrochemical properties[9,10] of the passive film formed on the UNS N07718 alloy in acidic solutions. Zhang *et al.*

reported that the passive film, formed on the surface of additively manufactured UNS N07718 in sulfuric acid, mainly consists of chromium oxide.[2] Luo *et al.* showed that an electrochemically resistive passive film is formed after solution heat treatment is applied on a selectively-laser-melted surface of UNS N07718 in an NaCl solution.[9] Amirjan *et al.* suggested that the scan rate during the additive manufacturing process affects the charge-transfer resistance of the passive film formed on UNS N07718 in an NaCl solution.[10]

The properties of the passive film formed on the surfaces of Fe–Cr–Ni alloys change over time. Some changes in the film, *i.e.*, thickness, chemical composition, electrochemical properties, and partial or entire degradation of the film, are related to localised corrosion. Fujimoto *et al.* reported that an increase in chromium composition in the passive film during electrochemical polarisation suppresses the initiation of localised corrosion on austenitic stainless steel.[11] Saito *et al.* suggested that the induction period is related to the thickness, composition, and electrochemical properties of the passive film formed on stainless steel in a neutral chloride solution.[12] Sugimoto *et al.* demonstrated that chloride ions decrease the thickness of the passive film formed on austenitic stainless steel, leading to its breakdown during the passivation.[13] Vignal *et al.* revealed that long-term electrochemical ageing of the passive film results in a less defective amorphous oxide film on duplex stainless steel.[14] Usually, ageing of the passive film formed on stainless steel enhances the localised corrosion resistance, because of the depletion of defects in the film, in a chloride-free environment.[15–17] In a neutral chloride solution, the Cr/Fe ratio and film thickness gradually increase during the ageing

[a]School of Materials Science and Engineering, Changwon National University, 51140 Changwondaehak-ro, Changwon, 51140, South Korea. E-mail: junseoblee@changwon.ac.kr; Fax: +82-55-261-7017; Tel: +82-55-213-3691

[b]Department of Materials Convergence and System Engineering, Changwon National University, 51140 Changwondaehak-ro, Changwon, 51140, South Korea

[c]R&d Center, SeAH CSS Corporation, Jeokhyun-ro, Changwon, 51708, South Korea

[d]Research Institute of Industry Science & Technology, Cheongam-ro, Pohang, 37673, South Korea

of the passive film formed on austenitic and duplex stainless steels.[18,19] Wang *et al.* revealed that the pre-passivated UNS S31603 surface in sulfuric acid blocks the chloride ions during the ageing of the film in an acidic chloride solution.[20] According to these reported studies, changes in the chemical composition of the film enhance the localised corrosion resistance of stainless steel in chloride-containing solutions.[18–22]

A comparison between the passivity of stainless steel and that of UNS N07718 reveals lack of sufficient information on the passive behaviour of UNS N07718. However, the changes in the composition, thickness and electrochemical properties of the passive film formed on the surface of UNS N07718 over time have not yet been reported. From a scientific and valuable perspective, it is important to comprehend how UNS N07718's passive film properties vary as it ages. Therefore, it is essential to understand the effect of variations in film composition, thickness and electrochemical properties of UNS N07718 over time. Furthermore, this information will aid in elucidating the localised corrosion behaviour of the alloy in corrosive environments. This study was focused on the evaluation of changes in the properties of the passive film formed on UNS N07718 in an acidic chloride solution, using electrochemical and surface analytical techniques.

2. Experimental

2.1. Materials preparation

The UNS N07718 (SeAH CSS Corp.) alloy was prepared in the form of a rod (diameter: 26 mm) with a chemical composition of 19.3 wt% Fe, 18.4 wt% Cr, 5.2 wt% Nb, 2.9 wt% Mo and 0.8 wt% Ti and Ni-balance. The rod was solution heat treated at 1050 °C for 2.5 h and then water quenched. Finally, the solution-treated specimen was aged at 780 °C for 8 h and air-cooled.

2.2. Electrochemical measurements

A three-electrode system, containing a platinum plate with a surface area of 10 cm^2 (counter electrode), an Ag/AgCl electrode immersed in saturated KCl (reference electrode; silver–silver chloride reference electrode; SSE), and UNS N07718 with an area of 1 cm^2 (working electrode), was employed for the electrochemical measurements. The UNS N07718 specimen was embedded in epoxy resin after being soldered with a copper wire using an Sn wire and was ground using a 600-grit SiC paper.

The working electrode was anodically polarised from −0.05 V, based on the rest potential, to the potential until the current density reached 5 mA cm^{-2} with a scan rate of 0.167 mV s^{-1}. After monitoring the electrode potential for 3600 s, the working electrode was polarised at 0.5 V$_{SSE}$ for 12 h. Electrochemical impedance spectroscopy (EIS) and Mott–Schottky (M–S) analysis were carried out for examining the UNS N07718 surface after polarisation at 0.5 V$_{SSE}$ for 300 s (5 min), 3600 s (1 h), 21 600 s (6 h) and 43 200 s (12 h). In the EIS analysis, the electrode potential was applied at 0.5 V$_{SSE}$ in the frequency range from 10^5 Hz to 10^{-2} Hz with a ±10 mV amplitude. In the M–S analysis, the electrode potential was changed from 0.5 V$_{SSE}$ to −1.0 V$_{SSE}$ at a rate of 50 mV s^{-1} and 10 Hz. All the

electrochemical measurements were performed in a deaerated solution containing 5 wt% NaCl + 0.5 wt% CH$_3$COOH at room temperature.

2.3. Surface analyses

After mirror-polishing by a 1 μm diamond suspension, the surface of the UNS N07718 specimen was polarised at 0.5 V$_{SSE}$ for 300, 3600, 21 600 and 43 200 s and analysed by X-ray photoelectron spectroscopy (XPS; VG SCIENTIFIC, NOVA). In the XPS analysis, a sample area with a diameter of 1 mm was illuminated by monochromatic Al Kα radiation (210 W, 15 kV, 14 mA). The depth profile was recorded by Ar$^+$ sputtering performed at a rate of 0.125 nm s^{-1}; Ta$_2$O$_5$ was used as the reference material for the depth profiling. The carbon C 1s peak at 285.0 eV, originating from carbon contamination, was used as the reference peak for deconvoluting the spectra.

3. Results and discussion

Fig. 1 shows the cyclic potentiodynamic polarisation curve of UNS N07718 in 5 wt% NaCl + 0.5 wt% CH$_3$COOH. The alloy surface does not exhibit an active-to-passive transition, indicating that the surface is immediately passivated in the experimental solution. From the corrosion potential to 0.7 V$_{SSE}$, the anodic current increases from *ca.* 0.01 μA cm^{-2} to reach a stable passive current density lower than *ca.* 2 μA cm^{-2}. At potentials >0.7 V$_{SSE}$, the anodic current increases and peaks *ca.* 30 μA cm^{-2} at 0.9 V$_{SSE}$, which indicates further oxidation reactions on the alloy surface. These oxidation reactions reportedly represent secondary oxidation of metallic elements (Cr, Fe or Ni) or metal cations on the surface of Ni–Cr–Fe alloys in acidic solutions.[23–25] At potentials >0.9 V$_{SSE}$, the anodic current decreases owing to the secondary passivation of the alloy surface. At potentials >1.1 V$_{SSE}$, the anodic current increases until 5 mA cm^{-2}, then decreases to its value obtained at the applied potential and reverses negative potential direction towards the corrosion potential. During the reverse scan, the reverse curve intersects the forward curve at *ca.* 0.95 V$_{SSE}$, which represents the
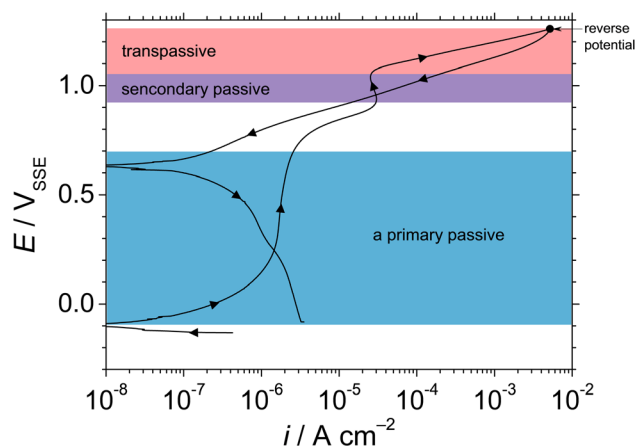

Fig. 1 Cyclic potentiodynamic polarisation curve of UNS N07718 in 5 wt% NaCl + 0.5 wt% CH$_3$COOH.
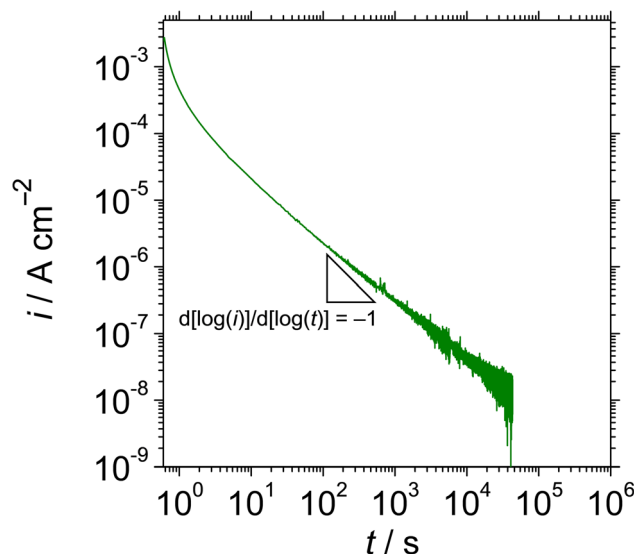
Fig. 2 Double logarithmic plot of current density with time at 0.5 V_{SSE} for UNS N07718 in 5 wt% NaCl + 0.5 wt% CH_3COOH.

repassivation potential for the secondary passivation on the alloy surface. Since the repassivation potential for the secondary passive state is higher than the primary passive region from the corrosion potential to *ca.* 0.7 V_{SSE}, the UNS N07718 surface remained in a stable primary passive state without the passive film breakdown in the experimental solution.

Fig. 2 shows the double logarithmic plot of current density with time at 0.5 V_{SSE} for UNS N07718 in 5 wt% NaCl + 0.5 wt% CH_3COOH. The current gradually decreases as the polarisation time increases, up to a slope of −0.85 for 10 s, demonstrating that the passive oxide grows through the consumption of the ionic current, based on the high-field mechanism,[26] on the alloy surface. After 10 s of polarisation, the current decreases to <80 nA cm^{-2}, and a slope of −0.85 is maintained for 43 200 s, indicating that the passive oxide formation is sustained during the polarisation.

Fig. 3 shows (a) Bode and (b) Nyquist plots of UNS N07718 polarised at 0.5 V_{SSE} for 300, 3600, 21 600 and 43 200 s in 5 wt%

NaCl + 0.5 wt% CH_3COOH. The resistance and phase shift values are fitted with the equivalent electronic circuit model, CPE-R_{ct}–R_s, where CPE is the constant phase element, and R_{ct} and R_s are the charge-transfer and solution resistances, respectively. The CPE is converted into interfacial capacitance C, which includes the capacitance of the Helmholtz and space-charge layers, by using the following equation:

$$C = Y_0^{\frac{1}{\alpha}} \left(\frac{1}{R_s} + \frac{1}{R_{ct}} \right)^{\frac{(\alpha-1)}{\alpha}}, \quad (1)$$

where Y_0 is the CPE constant, and α is the symmetric angle constant of the loop. The Kramer–Kronig transformation condition is satisfied at most frequencies. The Kramers–Kronig transformation is a mathematical relation between the imaginary and real components of responses obtained from a system that complies with certain assumptions. The relevant responses in EIS are the real and imaginary parts, or the phase and magnitude, of the impedance at a specific frequency. The real part can be calculated using Kramers–Kronig transformations if the imaginary part is known across the entire frequency range. Similarly, if the real part is known across the entire frequency range, it is possible to calculate the imaginary part. The phase shift values are close to −85° at a frequency lower than 100 Hz, indicating that the capacitive property of the alloy surface is dominant during the polarisation. R_{ct} increases, while C is almost constant, during the polarisation, suggesting that the polarisation makes the alloy surface electrically resistive (Fig. 4 and Table 1).

Fig. 5 shows the M–S plot of UNS N07718 polarised at 0.5 V_{SSE} for 300, 3600, 21 600 and 43 200 s in 5 wt% NaCl + 0.5 wt% CH_3COOH. The capacitance is obtained at a frequency of 10 Hz, as shown in Fig. 3, and includes the capacitances of the Helmholtz and space-charge layers:

$$\frac{1}{C} = \frac{1}{C_H} + \frac{1}{C_{SC}}, \quad (2)$$

where C_H and C_{SC} represent the capacitances of the Helmholtz and space-charge layers, respectively. Because the value of C_H is greater than that of C_{SC}, C is close to C_{SC}. The M–S equation of a semiconductive oxide is expressed as follows:
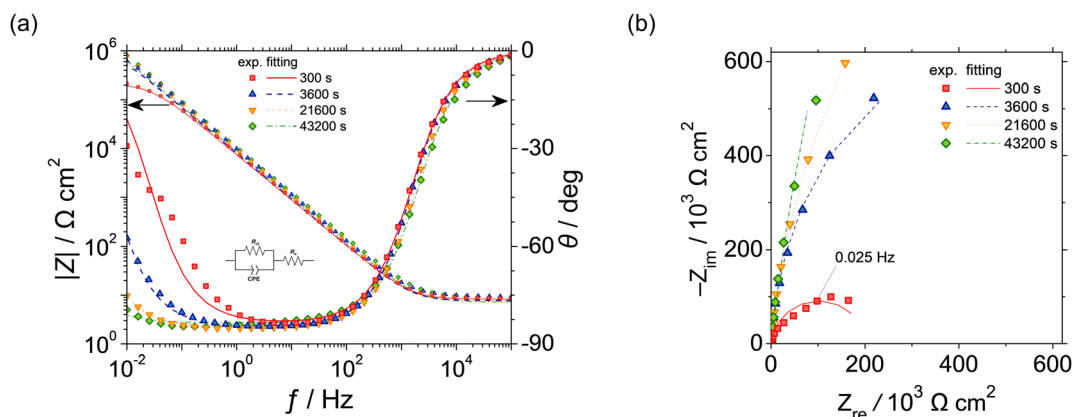

Fig. 3 (a) Bode and (b) Nyquist plots of UNS N07718 polarised at 0.5 V_{SSE} for 300, 3600, 21 600 and 43 200 s in 5 wt% NaCl + 0.5 wt% CH_3COOH.
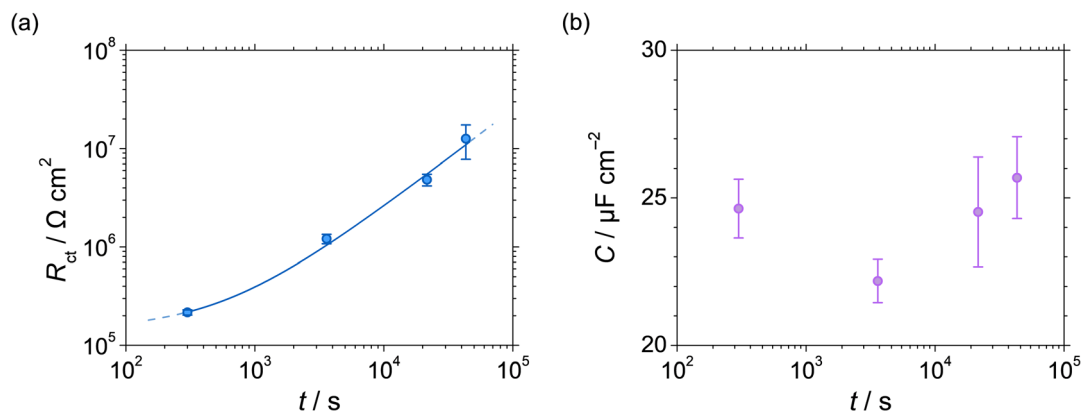
Fig. 4 (a) Charge-transfer resistance R_{ct} and (b) capacitance C at 0.5 V_{SSE} as functions of polarisation time of UNS N07718 in 5 wt% NaCl + 0.5 wt% CH$_3$COOH.

Table 1 Parameters obtained by fitting the EIS spectra

Polarisation time/s	R_s/Ω cm^2	$R_{ct}/10^6\ \Omega$ cm^2	C/μF cm^2
600	8.39 ± 0.19	0.22 ± 0.013	24.6 ± 1.00
3600	8.60 ± 0.83	1.21 ± 0.13	22.2 ± 0.73
21 600	7.73 ± 0.97	4.85 ± 0.66	24.5 ± 1.86
43 200	7.96 ± 0.69	12.6 ± 4.82	25.7 ± 1.39

$$\frac{1}{C_{SC}^2} = \left(\frac{1}{C} - \frac{1}{C_H}\right)^2 = \left(\frac{2}{\varepsilon\varepsilon_0 e N_D}\right)\left(E - E_{fb} - \frac{kT}{e}\right), \quad (3)$$

where ε is the dielectric constant; for n-type Cr hydroxides, $\varepsilon = 25$;[27] ε_0 is the permittivity constant in vacuum; e is the charge value; N_D is the donor density; E_{fb} is the flatband potential; k is Boltzmann's constant; and T is the absolute temperature. A decrease in the capacitance at potentials >0.4 V_{SSE} is observed because of the accumulation of charge carriers due to the flow of a non-faradaic current during an electrical time delay before the initiation of the M–S measurements. A positive slope is observed at potential <0.4 V_{SSE}, indicating that the alloy surface has n-type semiconductive characteristics. In acidic solutions of Ni-based alloy[28] and pure Cr,[29] an n-type surface oxide layer is formed, suggesting that chromium hydroxide is formed on the surface. Moreover, the p-type property of the Cr-oxide layer formed on Fe–Cr alloys in acidic solutions is evident from the negative slope observed the M–S plot at a potential <0.5 V_{SSE}.[30,31] However, when the potential shifts to negative potential values, which are lower than the corrosion potential, the passive layer can be damaged by cathodic reactions, such as reduction in film thickness or mechanical degradation by hydrogen evolution on the surface. This potential shift implies that it is difficult to identify the p-type property of the UNS N07718 surface at potentials <−0.1 V_{SSE}. Therefore, in this study, the capacitance is measured in the potential range of 0.5 V_{SSE} to −0.5 V_{SSE}. During the polarisation, the flatband potential (Fig. 6(a)) shifts towards the negative direction, and the donor density decreases (Fig. 6(b)), indicating that the passive oxide formed on the alloy surface becomes less defective.

Fig. 7 shows the XPS depth profiles of the UNS N07718 surface polarised at 0.5 V_{SSE} for (a) 300, (b) 3600, (c) 21 600, and (d) 43 200 s in 5 wt% NaCl + 0.5 wt% CH$_3$COOH. The presence of O with a high atomic concentration at the outer layer indicates that the alloy surface was covered with an oxide layer. An interface transition can be assumed between the oxide and the metal substrate, with an O concentration that is half of that of the maximum O concentration. Based on this assumption, the passive oxide film thickness is estimated as *ca.* 2 nm based on the sputter rate of reference Ta$_2$O$_5$ for 0.125 nm s^{-1}. Evidently, the atomic concentration of elemental Cr is higher than that of elemental Fe and Ni at the outermost layer of the film. The Cr atomic concentration is maximum at the interface between the oxide and the substrate and then gradually decreases, while that of Fe and Ni gradually increases as the sputtering time is increased. The photoelectron spectra obtained by X-ray irradiation contain depth information for a depth of *ca.* 2 nm on the surface, including that of the oxide film as well as the metallic substrate. As the sputtering time increases, the population of the
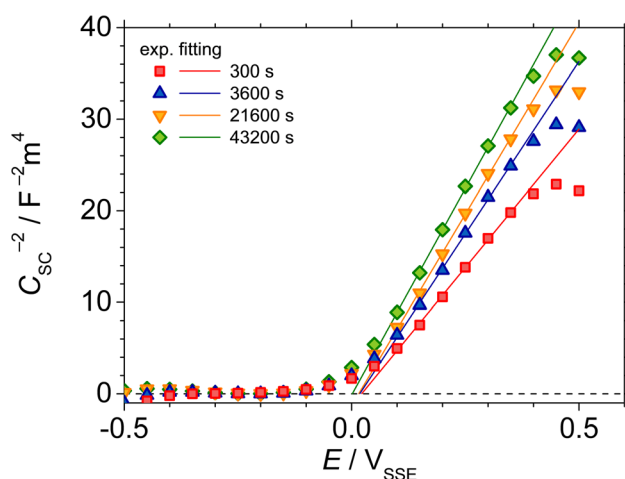

Fig. 5 M–S plots of UNS N07718 polarised at 0.5 V_{SSE} for 300, 3600, 21 600 and 43 200 s in 5 wt% NaCl + 0.5 wt% CH$_3$COOH.
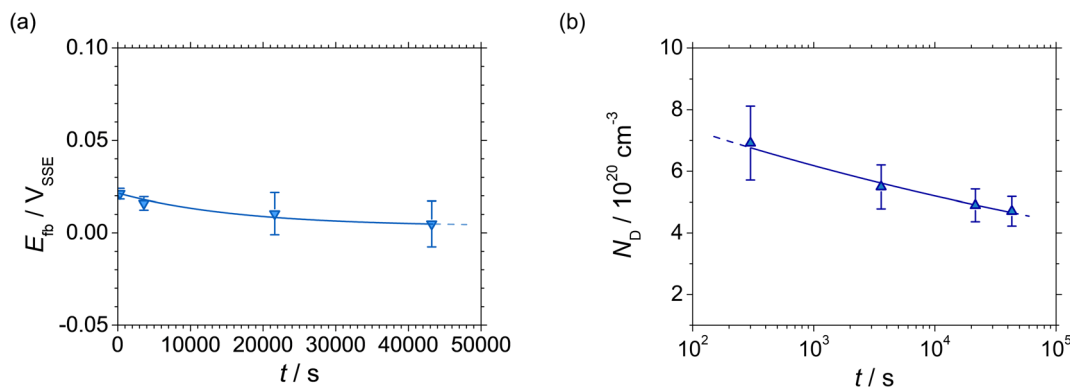
Fig. 6 (a) Flatband potential E_{fb}, and (b) donor density N_D at 0.5 V_{SSE} as functions of polarisation time of UNS N07718 in 5 wt% NaCl + 0.5 wt% CH_3COOH.

photoelectrons emitted from the metallic state increase, suggesting that the photoelectrons emitted by O indicate the oxidation state of the oxide, and the thickness of the film can be estimated from this information. After each polarisation time, the XPS depth profiles corresponding to the atomic concentration show similar behaviours, indicating that the compositional ratios of the elements in the film remain similar. Fig. 8 shows the passive film thickness calculated from the XPS depth profiles of the alloy surface during the polarisation at 0.5 V_{SSE}. The film thickness is almost constant at *ca.* 2 nm during the polarisation, indicating that the thickness of the passive film does not significantly change.

Fig. 9 shows the photoelectron spectra of (a) O 1s, (b) Cr $2p_{3/2}$, (c) Fe $2p_{3/2}$ and (d) Ni $2p_{3/2}$ for UNS N07718 polarised at 0.5 V_{SSE} for 300, 3600, 21 600, and 43 200 s in 5 wt% NaCl + 0.5 wt% CH_3COOH; in this case, the surface is not sputtered. The oxidation states of H_2O, OH^- and O^{2-} for oxygen, those of Cr^{3+} (hydroxide), Cr^{3+}(oxide) and Cr^0 for chromium, those of Fe^{3+}, Fe^{2+} and Fe^0 for iron, and those of Ni^{2+} and Ni^0 for nickel can be identified in the spectra. After Shirley background subtraction from narrow-scan spectra, the spectra are deconvoluted into individual spectrum corresponding to the oxidation states of oxygen, chromium, iron and nickel using the XPS peak binding energies shown in Table 2. The spectra of Mo 3d are not analysed
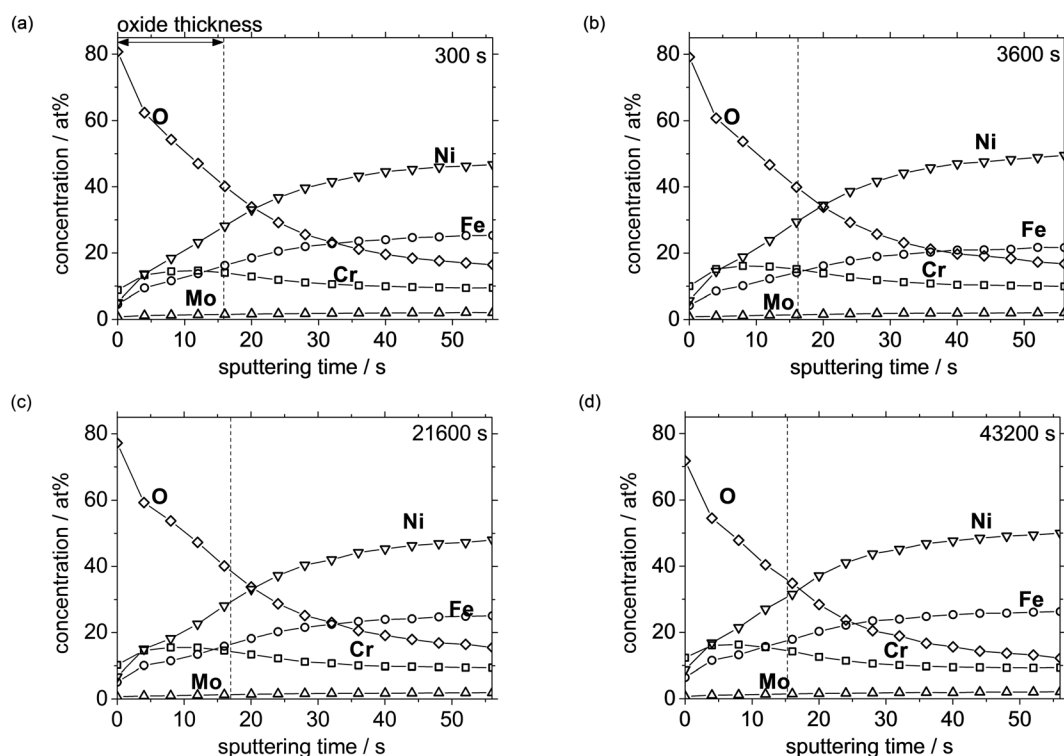

Fig. 7 XPS depth profile of UNS N07718 polarised at 0.5 V_{SSE} with polarisation time of (a) 300, (b) 3600, (c) 21 600 and (d) 43 200 s in 5 wt% NaCl + 0.5 wt% CH_3COOH.

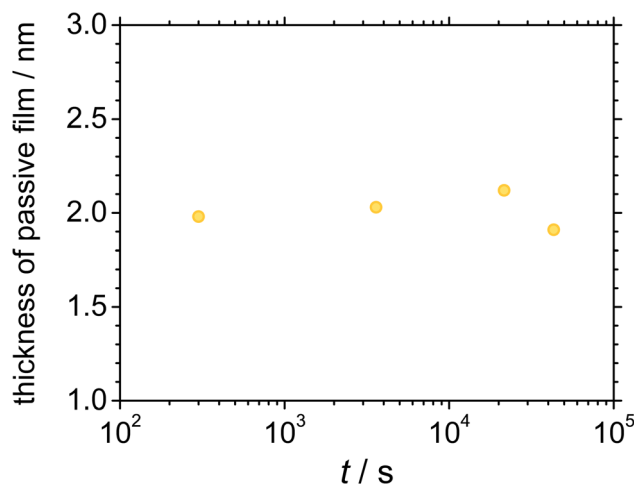Fig. 8 Estimated thickness of the passive film as a function of polarisation time at 0.5 V_{SSE}.

Table 2 Parameters for deconvolution of XPS spectra

Element	Peak	Binding energy, eV		Ref.
Fe	$2p_{3/2}$	Fe^0	707.1	32 and 33
		Fe^{2+}	708.5	34 and 35
		Fe^{3+}	711.8	36 and 37
Cr	$2p_{3/2}$	Cr^0	574.3	38 and 39
		Cr^{3+}(oxide)	576.2	38–40
		Cr^{3+}(hydroxide)	577.3	38 and 39
Ni	$2p_{3/2}$	Ni^0	852.8	36 and 41
		Ni^{2+}	855.6	37, 42 and 43
O	1s	O^{2-}	530.2	35–39
		OH^-	531.7	36, 39 and 43
		H_2O	532.5	44

owing to their low intensities. Because deconvoluting the spectrum of 2p orbital is complicated, in this study, the $2p_{3/2}$ spin data were used.

Fig. 10 shows the peak intensity ratios hydroxide/O^{2-}; M/(Cr^{3+}(hydroxide) + Cr^{3+}(oxide) + Cr^0), where M = Cr^{3+}(hydroxide) or Cr^{3+}(oxide); N/(Fe^{2+} + Fe^{3+} + Fe^0), where N = Fe^{2+} or Fe^{3+}; and Ni^{2+}/(Ni^{2+} + Ni^0) in each spectrum of the polarised surfaces. For all the polarisation durations of the surfaces (Fig. 10(a)), the hydroxide/O^{2-} ratio is higher at the outermost layer of the film, and the ratio gradually decreases as the sputtering time increases. Further, the hydroxide/O^{2-} ratio of the passive film decreases when the polarisation increases. It is presumed that the hydroxide layer is formed on the outermost layer of the passive film, and the hydroxide becomes an oxide in the film during the polarisation. The Cr^{3+}(hydroxide)/(Cr^{3+} (hydroxide) + Cr^{3+}(oxide) + Cr^0) and Fe^{3+}/(Fe^{2+} + Fe^{3+} + Fe^0) ratios are higher than the Cr^{3+}(oxide)/(Cr^{3+}(hydroxide) + Cr^{3+}(oxide) + Cr^0) and Fe^{3+}/(Fe^{2+} + Fe^{3+} + Fe^0) ratios at the outermost layer of the film, while the Cr^{3+}(hydroxide)/(Cr^{3+} (hydroxide)+Cr^{3+}(oxide)+Cr^0) and Fe^{3+}/(Fe^{2+} + Fe^{3+} + Fe^0) ratios decrease with the sputtering time. Moreover, the Cr^{3+}(hydroxide)/(Cr^{3+}(hydroxide) + Cr^{3+}(oxide) + Cr^0) and Fe^{3+}/(Fe^{2+} + Fe^{3+} + Fe^0) ratios gradually decrease in the film with the increasing polarisation time (Fig. 10(b) and (c)). The Ni^0/(Ni^{2+} + Ni^0) ratio is greater than Ni^{2+}/(Ni^{2+} + Ni^0)
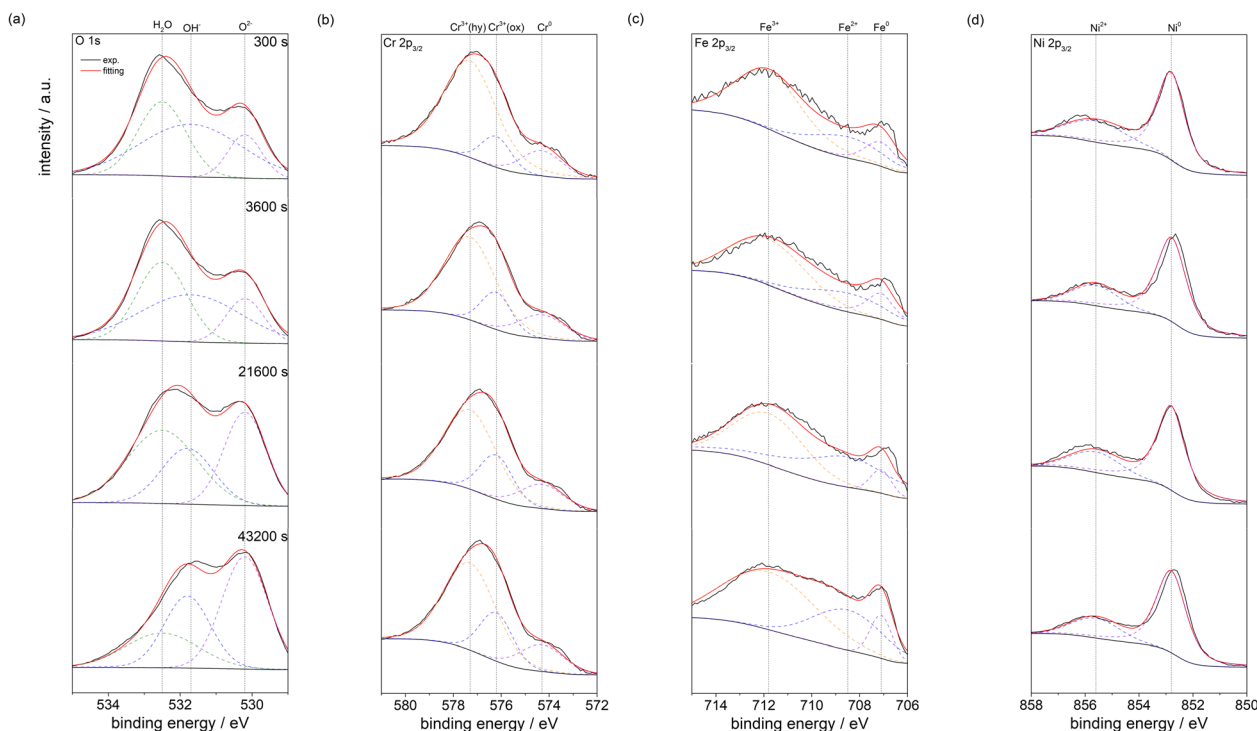

Fig. 9 Photoelectron spectra of (a) O 1s, (b) Cr $2p_{3/2}$, (c) Fe $2p_{3/2}$ and (d) Ni $2p_{3/2}$ obtained for UNS N07718 polarised at 0.5 V_{SSE} with polarisation time of 300, 3600, 21 600 and 43 200 s in 5 wt% NaCl + 0.5 wt% CH_3COOH.
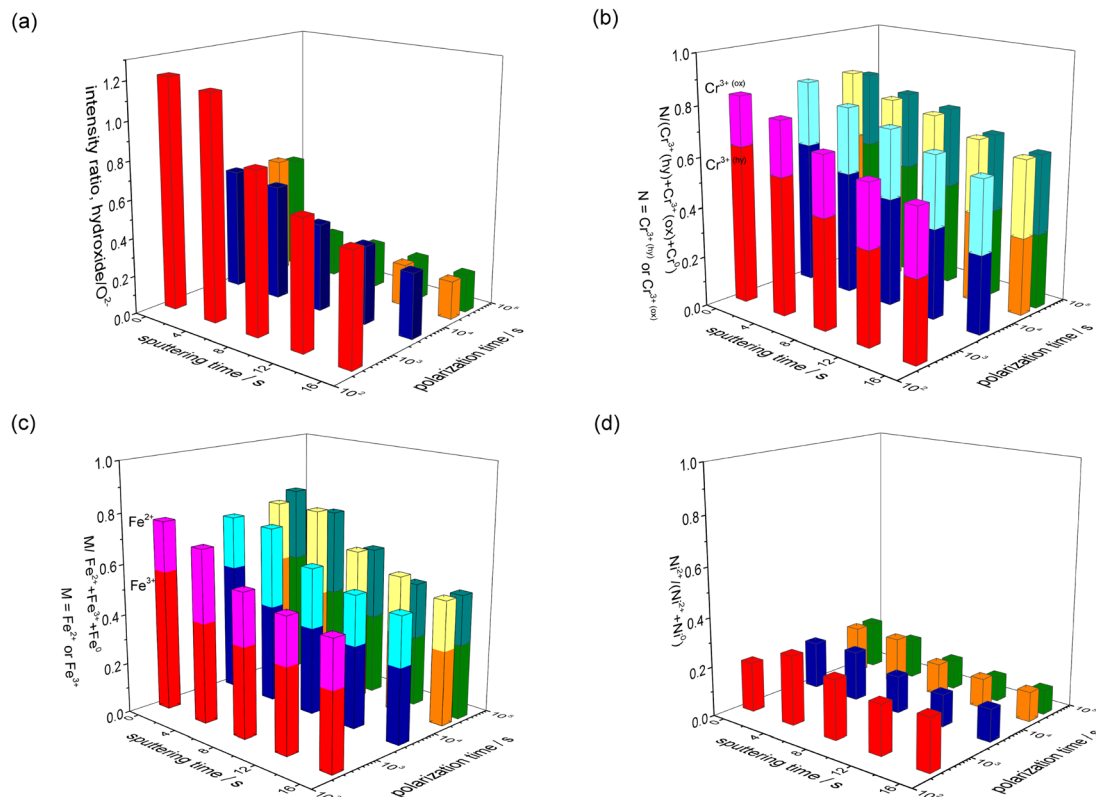
Fig. 10 Peak intensity ratio of the oxidation states of the elements (a) O (b) Cr (c) Fe and (d) Ni, present in the passive film, as a function of polarisation time.

ratio irrespective of the polarisation time (Fig. 10(d)), indicating that the Ni cation is a minor component in the passive film.

The XPS results reveal that the passive film formed on UNS N07718 is composed of a Cr-(hydro)oxide and Fe-oxide layer followed by an outer and inner layer enriched with Cr-hydro/oxide and Fe oxide, respectively. During the ageing, the Cr hydroxide in the outer layer of the film changes to a Cr-oxide layer, while the thickness of the film is almost constant at *ca.* 2 nm (Fig. 11). Elemental Cr is reportedly enriched in the passive film formed on the additively-manufactured UNS N07718 surface in sulfuric acid.[2] However, the structure of the oxide layer as the inner (or outer) layer of the film has not been elucidated.

The passive film formed on UNS N07718 becomes electrically resistive with a decrease in the defect density during the polarisation. The film exhibits n-type characteristics with a space-charge layer thickness of <1 nm, as evident from the M–S plot. This result is obtained by assuming that the semiconductive property, revealed from the electrochemical experiments, is strongly related to the Cr hydro/oxide and Fe oxide in the film. Since n-type semiconductors contain defects such as metal cationic interstitials and oxygen vacancies, the decrease in the defect density during the polarisation is believed to be mainly associated with the increase in the oxide concentration in the film:

$$M–OH = M–O + H^+ + e \qquad (4)$$
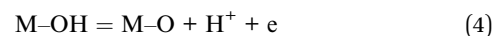
where M is a metal (Cr, Fe or Ni). During the polarisation, the dehydrated oxide layer, without the growth of the film, becomes electrochemically less reactive.
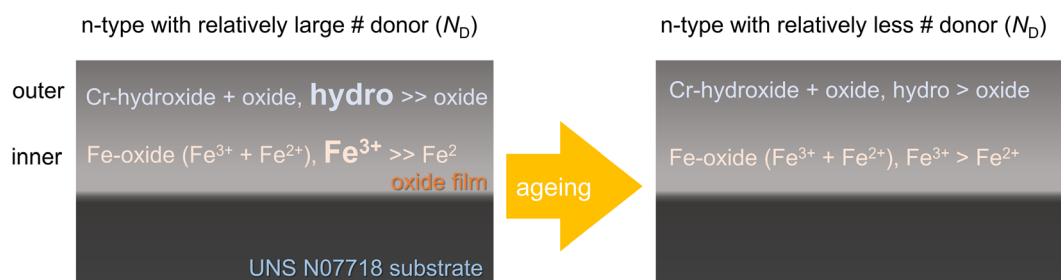

Fig. 11 Schematic illustration for the ageing of passive film formed on UNS N07718.

For Fe–Cr–Ni alloys, the passive film contains Fe oxide and Cr oxide at the outer and inner layers.[18–20] When the film comes in contact with Cl^-, Cl^- is adsorbed on the Fe-oxide layer of the film, and Fe–Cl complexes are formed. The complex dissolves in the solution, and the film becomes thin. This phenomenon is known as the adsorption mechanism, which degrades the passive film.[44] Recently, Auger spectroscopic results have revealed that the thickness of a passive film formed on austenitic stainless steel decreases significantly in a concentrated Cl^- solution. The thinned film accelerates additional charge transfer from the surface states to the metallic substrate through the n-type conduction band edge of the film.[45] Compared with Fe-based alloys, Ni-based alloys are more resistant to localised corrosion in chloride-containing environments. The findings of the present study demonstrate that the passive film formed on the UNS N07718 surface has Cr oxide and Fe oxide in its outer and inner layers. When UNS N07718 comes in contact with Cl^-, Cr–Cl complexes might form because of the adsorption of Cl^- on the Cr-oxide layer. These Cr–Cl complexes are insoluble, while the Fe–Cl complexes, *i.e.* $FeCl_2$ and $FeCl_3$, are soluble; up to 65.0 g of $FeCl_2$ and 91.2 g of $FeCl_3$ can be completely dissolved in 0.1 L of water.[46] It is speculated that the film formed on the UNS N07718 surface, enriched in Cr oxide at the outer layer, suppresses the degradation of the film in Cl-containing solutions, and this minimised degradation is related to the localised corrosion resistance of UNS N07718.

4. Conclusion

The ageing of the passive film on UNS N07718 was investigated in a shallow sour condition of 5 wt% NaCl + 0.5 wt% CH_3COOH. The UNS N07718 surface was in a passive state during polarisation at 0.5 V_{SSE} in the solution for 12 h, and the passive film formed on the alloy became relatively stable owing to the formation of an electrochemically resistive n-type oxide layer with less defects. XPS analysis revealed that the film comprised Cr- and Fe-enriched hydro/oxide outer and inner layers. Moreover, the film sustained its thickness at *ca.* 2 nm during the polarisation, while the outer Cr-hydroxide layer changed into a Cr-oxide layer. The first investigation of the passivation behaviour of UNS N07718 over polarisation time revealed that the passive surface maintained its passive state during the polarisation because the dehydrated oxide layer produced during the polarisation could change into a resistive and less-defective passive film.

Author contributions

Jun-Seob Lee: conceptualization; formal analysis; funding acquisition; investigation; methodology; project administration; supervision; Validation; Writing – original draft; writing – review & editing, Ye-Jin Lee: methodology; data curation; formal analysis; validation, Soon il Kwon: data curation; resources, Jungho Shin: resources; project administration, Sung Kang: data curation, funding acquisition; Seung-Hoon Baek: data curation; formal analysis, Je-Hyun Lee: project administration; funding acquisition.

Conflicts of interest

There are no conflicts to declare.

Acknowledgements

References

1 C.-M. Kuo, Y.-T. Yang, H.-Y. Bor, C.-N. Wei and C.-C. Tai, *Mater. Sci. Eng.*, 2009, **510**, 289.

2 L. N. Zhang and O. A. Ojo, *J. Alloys Compd.*, 2020, **829**, 154455.

3 B. Zhang, M. Xiu, Y. T. Tan, J. Wei and P. Wang, *Appl. Surf. Sci.*, 2019, **490**, 556.

4 H. S. Klapper and J. Stevens, *Corrosion*, 2014, **70**, 899.

5 Z. F. Yin, W. Z. Zhao, W. Y. Lai and X. H. Zhao, *Corros. Sci.*, 2009, **51**, 1702.

6 U. Martin, J. Ress, J. Bosch and D. M. Bastidas, *Metals*, 2020, **10**, 204.

7 G. A. Rao, M. Kumar, M. Srinivas and D. S. Sarma, *Mater. Sci. Eng. A*, 2003, **355**, 114.

8 X. L. An, L. Zhou, B. Zhang, J. J., C. L. Chu, L. Y. Han, H. G. Y. and P. K. Chu, *Mater. Res. Express*, 2019, **6**, 075803.

9 S. Luo, W. Huang, H. Yang, J. Yang, Z. Wang and X. Zeng, *Addit. Manuf.*, 2019, **30**, 100875.

10 M. Amirjan, M. Bozorg and H. Sakiani, *Mater. Chem. Phys.*, 2021, **263**, 124368.

11 S. Fujimoto, T. Yamada and T. Shibata, *J. Electrochem. Soc.*, 1998, **145**, L79.

12 H. Saito, T. Shibata and G. Okamoto, *Corros. Sci.*, 1979, **19**, 693.

13 K. Sugimoto, S. Matsuda, Y. Ogiwara and K. Kitamura, *J. Electrochem. Soc.*, 1985, **132**, 1791.

14 V. Vignal, H. Krawiec, O. Heintz and D. Mainy, *Corros. Sci.*, 2013, **67**, 109.

15 T. Ohtsuka, M. Ueda and M. Abe, *J. Electrochem. Soc.*, 2016, **163**, C459.

16 M. E. Curley-Fiorino and G. M. Schmid, *Corros. Sci.*, 1980, **20**, 313.

17 K. Oh, S. Ahn, K. Eom, K. Jung and H. Kwon, *Corros. Sci.*, 2014, **79**, 34.

18 R. Devaux, D. Vouagner, A. M. D. Becdelievre and C. Duret-Thual, *Corros. Sci.*, 1994, **36**, 11.

19 V. Vignal, H. Zhang, O. Delrue, O. Heintz, I. Popa and J. Peultier, *Corros. Sci.*, 2011, **53**, 894.

20 Z. Wang, A. Seyeux, S. Zanna, V. Maurice and P. Marcus, *Electrochim. Acta*, 2020, **329**, 135159.

21 Y. Qiao, X. Wang, L. Yang, X. Wang, J. Chen, Z. Wang, H. Zhou, J. Zou and F. Wang, *J. Mater. Sci. Technol.*, 2022, **107**, 197.

22 Y. Zhang, J. Yu, X. L. P. Guo, X. Yu, S. Zhang, J. Liu and W. Huang, *Corros. Sci.*, 2022, **205**, 110439.

23 J. R. Myers, F. H. Beck and M. G. Fontana, *Corrosion*, 1956, **21**, 277.

24 M. Bojinov, I. Betova, G. Fabricius, T. Laitinen, R. Raicheff and T. Saario, *Corros. Sci.*, 1999, **41**, 1557.

25 C. T. Liu and J. K. Wu, *Corros. Sci.*, 2007, **49**, 2198.

26 N. Cabrera and N. F. Mott, *Rep. Prog. Phys.*, 1949, **12**, 163.

27 T. P. Moffat and R. M. Latanision, *J. Electrochem. Soc.*, 1992, **130**, 1869.

28 J.-S. Lee and R. Bäßler, *Corros. Eng., Sci.*, 2018, **53**, 302.

29 Ž. Petrović, N. Lajçi, M. Metikoš-Huković and R. Babić, *J. Solid State Electrochem.*, 2011, **15**, 1201.

30 N. Zakerin and K. Morshed-Behbahani, *Metall. Mater. Trans. A*, 2021, **52**, 3247.

31 J. Huang, X. Wu and E.-H. Han, *Corros. Sci.*, 2009, **51**, 2976.

32 A. S. Lim and A. Atrens, *Appl. Phys. A*, 1990, **51**, 411.

33 R. Idczak, K. Idczak and R. Konieczny, *Corrosion*, 2018, **74**, 623.

34 N. S. McIntyre and D. G. Zetaruk, *Anal. Chem.*, 1977, **49**, 1521.

35 T. L. Barr, *J. Phys. Chem.*, 1978, **82**, 1801.

36 J. Chastain, and R. C. King Jr, *Handbook of X-ray photoelectron spectroscopy*, Perkin-Elmer Corporation, 1992, vol. 40, p. 221.

37 B. Stypula and J. Stoch, *Corros. Sci.*, 1994, **36**, 2159.

38 M. C. Biesinger, C. Brown, J. R. Mycroft, R. D. Davidson and N. S. McIntyre, *Surf. Interface Anal.*, 2004, **36**, 1550.

39 A. Lebugle, U. Axelsson, R. Nyholm and N. Mårtensson, *Phys. Scr.*, 1981, **23**, 825.

40 I. Olefjord, B. Brox and U. Jelvestam, *J. Electrochem. Soc.*, 1985, **132**, 2854.

41 N. S. McIntyre and M. G. Cook, *Anal. Chem.*, 1975, **47**, 2208.

42 C. E. Dubé, B. Workie, S. P. Kounaves, A. Robbat Jr, M. L. Aksub and G. Davies, *J. Electrochem. Soc.*, 1995, **142**, 3357.

43 S. Jin and A. Atrens, *Appl. Phys. A*, 1987, **42**, 149.

44 J. M. Kolotyrkin, *Corrosion*, 1963, **19**, 261t.

45 J.-S. Lee, T. Kawano, T. Ishii, Y. Kitagawa, T. Nakanishi, Y. Hasegawa and K. Fushimi, *J. Electrochem. Soc.*, 2017, **164**, C1.

46 D. R. Lide, *CRC Handbook of Chemistry and Physics*, CRC Press, Boca Raton, 9th edn, 2010, vol. 4, pp. 58–69.